Exponential Attitude-Orbit Coordinated Control for Gravitational-Wave Detection Spacecraft Formation with Large-Scale Communication Delays

XING Youpeng, SONG Yinsheng, YIN Zeyang, CHEN Xiaofang*

School of Automation, Central South University, Changsha 410083, P. R. China

(Received 30 October 2024; revised 8 January 2025; accepted 10 January 2025)

Abstract: This paper concerns the exponential attitude-orbit coordinated control problems for gravitational-wave detection formation spacecraft systems. Notably, the large-scale communication delays resulting from oversized inter-satellite distance of space-based laser interferometers are first modeled. Subject to the delayed communication behaviors, a new delay-dependent attitude-orbit coordinated controller is designed. Moreover, by reconstructing the less conservative Lyapunov-Krasovskii functional and free-weight matrices, sufficient criteria are derived to ensure the exponential stability of the closed-loop relative translation and attitude error system. Finally, a simulation example is employed to illustrate the numerical validity of the proposed controller for in-orbit detection missions.

Key words: gravitational-wave detection; spacecraft formation; attitude-orbit coordinated control; large-scale communication delays; exponential stability

CLC number: TN925 **Document code:** A **Article ID:** 1005-1120(2025)01-0070-10

0 Introduction

According to Einstein's general theory of relativity, gravitation affects the space-time curvature such that the variation of the latter propagates outward like ripples. Since the 1960s, it has been vital for the academic community to acquire evidence of gravitational waves through experiments[1-3]. By relevant detection missions, it may provide crucial clues for the origin and evolution of the universe. In 2015, the Laser Interferometer Gravitational-wave Observatory (LIGO) first detected gravitational waves on the ground[4]. However, there exist thorny noises and a limited scope of LIGO, which makes them mainly focus on wave sources with weaker intensity. For this, space-based gravitational-wave detection missions, such as Laser Interferometer Space Antenna (LISA)[5-6], Deci-hertz IGO[7], TianQin[8-9] and TaiJi[10] programs, and so on, can overcome the shortcomings of the ground-based ones and provide the capability to explore a wider wave frequency range. As a significant technique of such missions, the past decade has witnessed increasing interest in control research for multi-spacecraft systems. For example, Shi et al.[11] addressed the optimal tracking control problems for the leader-follower spacecraft formation system. Song et al.[12] presented the design validation for the small-scale magnetosphere and ionosphere plasma experiment mission. Wang et al.[13] investigated the coordinated control problems for spacecraft formation flying with obstacle and collision avoidance. It should be emphasized that there is still a lack of findings on the coordinated flying of formation spacecraft systems with gravitational-wave detection missions.

In practice, for a better scope of the detection, the spacecrafts equipped with laser interferometers are separated by an oversized distance, e.g., the designed distance 2.5×10^6 km in LISA. Nevertheless, the data transmission rate with the laser being

*Corresponding author, E-mail address: yinzeyang@csu.edu.cn.

How to cite this article: XING Youpeng, SONG Yinsheng, YIN Zeyang, et al. Exponential attitude-orbit coordinated control for gravitational-wave detection spacecraft formation with large-scale communication delays[J]. Transactions of Nanjing University of Aeronautics and Astronautics, 2025,42(1):70-79.

http://dx.doi.org/10.16356/j.1005-1120.2025.01.005

a carrier is restricted in the universe, and the propagation time of information for neighboring spacecrafts are approximately 8.33 s in LISA. When different spacecrafts cooperate through such large-scale delayed information for formation reconfiguration and maintenance, the overall control performance of flying formation may be degraded, and the entire multi-spacecraft systems may even become destabilized. Currently, lots of researchers studied the relevant problems of various objects with communication delays, e.g., the delayed attitude coordinated tracking for spacecraft formation with parametric uncertainties[14], the output consensus for heterogeneous multi-agent systems with nonuniform communication delays[15], and the synchronization for fuzzy memristive neural networks with time delay[16]. Especially, Zhang et al.[17] concentrated on the attitude and position delayed control issues for multi-spacecraft systems in TianQin, where spacecrafts work in geocentric orbit with communication distance $\sqrt{3}\times10^5$ km and fixed delays 0.67 s. Although the existing achievements can provide meaningful references when modeling delays, few of them dedicate such large-scale time-variant communication delays and the exponential stability of closed-loop delayed systems in theory or practice.

Motivated by the above discussion, a delay-dependent attitude-orbit coordinated control scheme is proposed for spacecraft formation with gravitational-wave detection missions. The prominent contributions are twofold.

The large-scale delayed communication behaviors among the heliocentric-orbit-based gravitational-wave detection spacecrafts are modeled for the first attempt, which facilitates the attitude-orbit coordinated controller design for spacecraft formation in this scenario.

A novel delay-dependent attitude-orbit coordinated controller is proposed to alleviate the negative effect of large-scale communication delays. To derive sufficient criteria ensuring that the closed-loop error system is exponentially stable with less conservativeness but more solution flexibility, a set of Lyapunov-Krasovskii functional containing the delay information and free-weight matrices are constructed.

The organization of this paper is as follows: In section 1, the concerned topics are formulated. In section 2, the delay-dependent attitude-orbit coordinated controller is suggested. An illustrative example is presented in section 3 to verify the numerical validity. Finally, section 4 summarizes this paper.

1 Problem Formulation

This paper focuses on the detection formation composed of N spacecrafts and a digraph describes their interaction.

1.1 Interaction graph

Denote a digraph $\boldsymbol{G}\triangleq\{B,E,\boldsymbol{A}\}$, where $B\triangleq\{n_i,i=1,2,\cdots,N\}$, $E\subseteq B\times B$, and $\boldsymbol{A}\triangleq[\alpha_{ij}]\in\mathbf{R}^{N\times N}$ are the node-set, the edge set and the adjacency matrix, respectively. The coefficients $\alpha_{ij}>0$. If the node i can receive information from node j, i.e., $\alpha_{ij}>0\Leftrightarrow(n_j,n_i)\in E$. Meanwhile, $\alpha_{ii}=0$ holds for $\forall i\in S\triangleq\{1,2,\cdots,N\}$. The in-degree of node i is obtained by $d_i\triangleq\sum_{j=1}^{N}\alpha_{ij}$, then the Laplacian matrix for $\boldsymbol{G}$ is defined as $\boldsymbol{L}\triangleq\boldsymbol{D}-\boldsymbol{A}$, in which $\boldsymbol{D}\triangleq\mathrm{diag}\{d_1,d_2,\cdots,d_N\}$. Besides, $\boldsymbol{G}$ contains a spanning tree throughout this paper.

1.2 Large-scale communication delay model

When the lasers are utilized as information carriers for inter-satellite interaction, the propagation distance is the primary factor for real-time communication behaviors, e.g., the propagation distance $\sqrt{3}\times10^5$ km and fixed delays 0.67 s in TianQin[17]. We have paid attention to the more challenging issues brought by larger communication distance 2.5×10^6 km and delays (approximate 8.33 s) in the LISA project. Moreover, other factors like hardware capabilities, and overloaded sensors caused by background light, etc., may also lead to delayed information delivery. To sum up, the large-scale communication delays $\tau(t)$ are reasonably modeled as

$$\begin{cases}\tau_1\leqslant\tau(t)\leqslant\tau_2\\ \dot{\tau}(t)\leqslant\gamma\end{cases}\tag{1}$$

where $0\leqslant\tau_1\leqslant\tau_2$ means that the delay signal $\tau(t)$ is bounded and γ the constant.

1.3 Spacecraft motion and attitude model

As shown in Fig.1, the inertial coordinate frame and the body-fixed one are set as O_{I} and O_{bi}, respectively. The ith spacecraft is abbreviated as C_i for $\forall i\in S$, and C_0 represents the virtual leader spacecraft at the geometric center of the formation. With C_0 being the origin, the local-vertical local-horizontal frame O_{L} is established to characterize the relative translation of gravitational-wave detection spacecraft. Therein, axis x_{L} is along with the direction of the position vector $\boldsymbol{\ell}_0$, axis z_{L} is perpendicular to the orbital plane of C_0, and axis y_{L} obeys the right-handed rules.

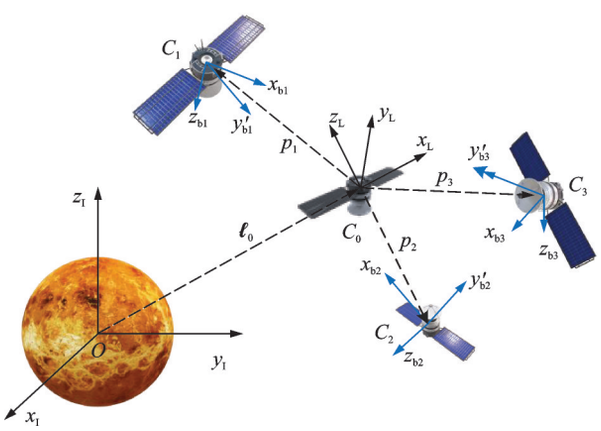

Fig.1 Architecture of gravitational-wave detection spacecraft formation

In O_{I}, the orbital dynamics of C_0 can be modeled as

$$\ddot{\boldsymbol{\ell}}_0=-\frac{c_{\mathrm{s}}}{\|\boldsymbol{\ell}_0\|^3}\boldsymbol{\ell}_0 \tag{2}$$

where $\boldsymbol{\ell}_0\in\mathbf{R}^3$ is the position vector of C_0, c_{s} the gravitational constant of Sun. For $\forall i\in S$, denote $\boldsymbol{p}_i\triangleq\boldsymbol{\ell}_i-\boldsymbol{\ell}_0$ and $\boldsymbol{p}_i\triangleq[x_i,y_i,z_i]^{\mathrm{T}}\in\mathbf{R}^3$ by the position vectors $\boldsymbol{\ell}_i$ of C_i. Then, in O_{L}, the relative translation of C_i is derived as

$$\begin{cases}\ddot{x}_i=\dot{\rho}^2x_i+\dfrac{c_{\mathrm{s}}}{R_0^2}-\dfrac{c_{\mathrm{s}}(R_0+x_i)}{R_i^3}+2\dot{y}_i\dot{\rho}+y_i\ddot{\rho}+u_{i,a,x}\\ \ddot{y}_i=\dot{\rho}^2y_i-\dfrac{c_{\mathrm{s}}}{R_i^3}y_i-2\dot{x}_i\dot{\rho}-x_i\ddot{\rho}+u_{i,a,y}\\ \ddot{z}_i=-\dfrac{c_{\mathrm{s}}}{R_i^3}z_i+u_{i,a,z}\end{cases} \tag{3}$$

where $\boldsymbol{u}_{i,a}\triangleq[u_{i,a,x},u_{i,a,y},u_{i,a,z}]^{\mathrm{T}}\in\mathbf{R}^3$ is the orbit control input; $R_i\triangleq\|\boldsymbol{\ell}_i\|$ for $i=0,1,\cdots,N$. Moreover, given the orbital eccentricity e_0 of C_0, the evolution of the true anomaly ρ satisfies

$$\begin{cases}\dot{\rho}^2=\dfrac{c_{\mathrm{s}}}{R_0^3}(1+e_0\cos\rho)\\ \ddot{\rho}=-2\dfrac{c_{\mathrm{s}}}{R_0^3}e_0\sin\rho\end{cases} \tag{4}$$

By setting the desired value $\boldsymbol{p}_{i,\mathrm{d}}$ for $\boldsymbol{p}_i$ and $\boldsymbol{\eta}_{i,1}\triangleq\boldsymbol{p}_i-\boldsymbol{p}_{i,\mathrm{d}}$, the relative translation error system is expressed as

$$\begin{cases}\dot{\boldsymbol{\eta}}_{i,1}=\boldsymbol{\eta}_{i,2}\\ \dot{\boldsymbol{\eta}}_{i,2}=\boldsymbol{f}(\boldsymbol{p}_i,\dot{\boldsymbol{p}}_i)+\boldsymbol{u}_{i,a}-\ddot{\boldsymbol{p}}_{i,\mathrm{d}}\end{cases} \tag{5}$$

where

$$\boldsymbol{f}(\boldsymbol{p}_i,\dot{\boldsymbol{p}}_i)\triangleq\begin{bmatrix}\dot{\rho}^2x_i+\dfrac{c_{\mathrm{s}}}{R_0^2}-\dfrac{c_{\mathrm{s}}(R_0+x_i)}{R_i^3}+2\dot{y}_i\dot{\rho}+y_i\ddot{\rho}\\ \dot{\rho}^2y_i-\dfrac{c_{\mathrm{s}}}{R_i^3}y_i-2\dot{x}_i\dot{\rho}-x_i\ddot{\rho}\\ -\dfrac{c_{\mathrm{s}}}{R_i^3}z_i\end{bmatrix} \tag{6}$$

Furthermore, for $\forall i\in S$, the attitude dynamic model of C_i in O_{bi} is provided as

$$\dot{\tilde{\boldsymbol{q}}}_{i,\mathrm{v}}=\frac{1}{2}\boldsymbol{Q}_{\mathrm{v}}(\tilde{\boldsymbol{q}}_i)\boldsymbol{\omega}_i \tag{7}$$

$$\dot{\tilde{q}}_{i,\mathrm{c}}=\frac{1}{2}\tilde{\boldsymbol{q}}_{i,\mathrm{v}}^{\mathrm{T}}\boldsymbol{\omega}_i \tag{8}$$

$$\boldsymbol{J}_i\dot{\boldsymbol{\omega}}_i=-\boldsymbol{\omega}_i^{\times}\boldsymbol{J}_i\boldsymbol{\omega}_i+\boldsymbol{u}_{i,b} \tag{9}$$

where the unit attitude quaternion $\tilde{\boldsymbol{q}}_i\triangleq[\tilde{\boldsymbol{q}}_{i,\mathrm{v}}^{\mathrm{T}},\tilde{q}_{i,\mathrm{c}}]^{\mathrm{T}}\in\mathbf{R}^4$ is used to depict the rotation from O_{I} to O_{bi}; $\boldsymbol{\omega}_i\in\mathbf{R}^3$ the angular velocity vector and $\boldsymbol{J}_i\in\mathbf{R}^{3\times3}$ the inertia matrix. $\boldsymbol{Q}_{\mathrm{v}}(\tilde{\boldsymbol{q}}_i)\triangleq\tilde{q}_{i,\mathrm{c}}\boldsymbol{I}_{3\times3}+\tilde{\boldsymbol{q}}_{i,\mathrm{v}}^{\times}\in\mathbf{R}^{3\times3}$ and the operator $\boldsymbol{a}^{\times}$ meets

$$\boldsymbol{a}^{\times}\triangleq\begin{bmatrix}0&-a_3&a_2\\ a_3&0&-a_1\\ -a_2&a_1&0\end{bmatrix}$$

with $\boldsymbol{a}\triangleq[a_1,a_2,a_3]^{\mathrm{T}}$; $\boldsymbol{u}_{i,b}\triangleq[u_{i,b,x},u_{i,b,y},u_{i,b,z}]^{\mathrm{T}}\in\mathbf{R}^3$ is the attitude control input.

After that, considering the desired attitude $\tilde{\boldsymbol{q}}_{i,\mathrm{d}}$ and the quaternion multiplication operator $\oplus$ defined in Ref.[18], the attitude error $\tilde{\boldsymbol{q}}_{i,\mathrm{e}}\triangleq[\tilde{\boldsymbol{q}}_{i,\mathrm{e,v}}^{\mathrm{T}},\tilde{q}_{i,\mathrm{e,c}}]^{\mathrm{T}}\in\mathbf{R}^4$ can be calculated by $\tilde{\boldsymbol{q}}_{i,\mathrm{e}}=\tilde{\boldsymbol{q}}_i\oplus\tilde{\boldsymbol{q}}^{-1}{}_{i,\mathrm{d}}$. Similar to Ref.[19], one can get the rotation matrix $\boldsymbol{C}_{i,\mathrm{e}}$ as

$$\boldsymbol{C}_{i,\mathrm{e}}=(\tilde{\boldsymbol{q}}_{i,\mathrm{e,c}}^2-\tilde{\boldsymbol{q}}_{i,\mathrm{e,v}}^{\mathrm{T}}\tilde{\boldsymbol{q}}_{i,\mathrm{e,v}})\boldsymbol{I}_{3\times3}+2\tilde{\boldsymbol{q}}_{i,\mathrm{e,v}}\tilde{\boldsymbol{q}}_{i,\mathrm{e,v}}^{\mathrm{T}}-2\tilde{\boldsymbol{q}}_{i,\mathrm{e,c}}\tilde{\boldsymbol{q}}_{i,\mathrm{e,v}} \tag{10}$$

Next, the angular velocity error $\boldsymbol{\omega}_{i,\mathrm{e}} \in \mathbf{R}^3$ is presented as

$$\boldsymbol{\omega}_{i,\mathrm{e}} = \boldsymbol{\omega}_i - \boldsymbol{C}_{i,\mathrm{e}}\boldsymbol{\omega}_{i,\mathrm{d}} \tag{11}$$

where $\boldsymbol{\omega}_{i,\mathrm{d}} \in \mathbf{R}^3$ is the desired value for $\boldsymbol{\omega}_i$.

Combining with $\dot{\boldsymbol{C}}_{i,\mathrm{e}} = -\boldsymbol{\omega}_{i,\mathrm{e}}^{\times}\boldsymbol{C}_{i,\mathrm{e}}$, it yields that

$$\dot{\boldsymbol{\omega}}_{i,\mathrm{e}} = \boldsymbol{g}(\tilde{\boldsymbol{q}}_{i,\mathrm{e}}, \dot{\tilde{\boldsymbol{q}}}_{i,\mathrm{e}}) + \boldsymbol{J}_i^{-1}\boldsymbol{u}_{i,b} \tag{12}$$

where

$$\boldsymbol{g}(\tilde{\boldsymbol{q}}_{i,\mathrm{e}}, \dot{\tilde{\boldsymbol{q}}}_{i,\mathrm{e}}) \triangleq -\boldsymbol{J}_i^{-1}\boldsymbol{\omega}_i^{\times}\boldsymbol{J}_i\boldsymbol{\omega}_i - \boldsymbol{C}_{i,\mathrm{e}}\dot{\boldsymbol{\omega}}_{i,\mathrm{d}} + \boldsymbol{\omega}_{i,\mathrm{e}}^{\times}\boldsymbol{C}_{i,\mathrm{e}}\boldsymbol{\omega}_{i,\mathrm{d}}$$

1.4 Control objective

A possible mission scenario for space-based gravitational-wave detection is shown in Fig.2. The constellation contains three spacecrafts operating in heliocentric orbits, and its center o located in the Earth's orbit lags the Earth by an approximately a 20° angle. The distance between C_i and its neighbor C_j is designed as 2.5×10^6 km. There are two identical interferometers equipped in C_i, and the axes passing through test mass (TM) intersect with a 60° angle.

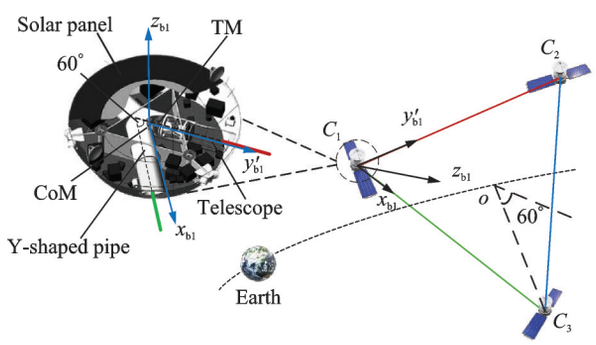

Fig.2 Orbit and constellation of detection spacecraft

The frame O_{bi} is established with the center of mass (CoM) of C_i. Taking C_1 as an example, x_{b1} and y'_{b1} are pointed to its target C_3 and neighbor C_2, respectively, and z_{b1} obeys the right-hand rules. It is crucial to track the desired configuration of gravitational-wave detection spacecraft for space-based laser interferometry. Inevitably, the interaction among formation members suffers from large-scale communication delays. Therefore, our control objective is to stabilize the relative translation and attitude error systems in this situation, namely, $\boldsymbol{\eta}_{i,1} \to 0$, $\boldsymbol{\eta}_{i,2} \to 0$, $\tilde{\boldsymbol{q}}_{i,\mathrm{e,v}} \to 0$, and $\boldsymbol{\omega}_{i,\mathrm{e}} \to 0$.

2 Main Results

In this section, we propose a novel delay-dependent attitude-orbit coordinated control scheme for gravitational-wave detection spacecraft systems. With the presence of large-scale communication delays $\tau(t)$, it will show that the exponential stabilization issue for the closed-loop error system is solvable with the utilization of sufficient conditions in Theorem 1.

2.1 Attitude-orbit coordinated controller design

For $\forall i \in S$, the closed-loop system can be divided into an orbit control loop and an attitude control loop. There is a nominal control part $\boldsymbol{u}_{i,s,1}$, two coordinated control parts $\boldsymbol{u}_{i,s,2}$ and $\boldsymbol{u}_{i,s,3}$ in each loop $(s = a, b)$.

With consideration of large-scale communication delays $\tau(t)$, the delay-dependent orbit coordinated controller $\boldsymbol{u}_{i,a}$ is designed in O_{L} as

$$\boldsymbol{u}_{i,a} \triangleq \boldsymbol{u}_{i,a,1} + \boldsymbol{u}_{i,a,2} + \boldsymbol{u}_{i,a,3} \tag{13}$$

where

$$\begin{cases} \boldsymbol{u}_{i,a,1} \triangleq -\boldsymbol{f}(\boldsymbol{p}_i, \dot{\boldsymbol{p}}_i) + \ddot{\boldsymbol{p}}_{i,\mathrm{d}} - \boldsymbol{\Lambda}_i\boldsymbol{\eta}_{i,2} - k_{i,a}(\boldsymbol{\Lambda}_i\boldsymbol{\eta}_{i,1} + \boldsymbol{\eta}_{i,2}) \\ \boldsymbol{u}_{i,a,2} \triangleq -\sum_{j=1}^{N}\alpha_{ij}(\boldsymbol{\Lambda}_i\boldsymbol{\eta}_{i,1}(t-\tau(t)) - \boldsymbol{\Lambda}_j\boldsymbol{\eta}_{j,1}(t-\tau(t))) \\ \boldsymbol{u}_{i,a,3} \triangleq -\sum_{j=1}^{N}\alpha_{ij}(\boldsymbol{\eta}_{i,2}(t-\tau(t)) - \boldsymbol{\eta}_{j,2}(t-\tau(t))) \end{cases}$$

$\boldsymbol{\Lambda}_i$ is a positive diagonal matrix and $k_{i,a}$ the orbit controller gain to be determined.

Correspondingly, the delay-dependent attitude coordinated controller $\boldsymbol{u}_{i,b}$ is designed in O_{bi} as

$$\boldsymbol{u}_{i,b} \triangleq \boldsymbol{u}_{i,b,1} + \boldsymbol{u}_{i,b,2} + \boldsymbol{u}_{i,b,3} \tag{14}$$

where

$$\begin{cases} \boldsymbol{u}_{i,b,1} \triangleq -\boldsymbol{J}_i\boldsymbol{g}(\tilde{\boldsymbol{q}}_{i,\mathrm{e}}, \dot{\tilde{\boldsymbol{q}}}_{i,\mathrm{e}}) - \dfrac{\boldsymbol{Q}_{i,\mathrm{e}}\boldsymbol{\omega}_{i,\mathrm{e}}}{2} - k_{i,b}(\boldsymbol{J}_i\boldsymbol{\omega}_{i,\mathrm{e}} + \tilde{\boldsymbol{q}}_{i,\mathrm{e,v}}) \\ \boldsymbol{u}_{i,b,2} \triangleq -\sum_{j=1}^{N}\alpha_{ij}(\boldsymbol{q}_{i,\mathrm{e,v}}(t-\tau(t)) - \boldsymbol{q}_{j,\mathrm{e,v}}(t-\tau(t))) \\ \boldsymbol{u}_{i,b,3} \triangleq -\sum_{j=1}^{N}\alpha_{ij}(\boldsymbol{J}_i\boldsymbol{\omega}_{i,\mathrm{e}}(t-\tau(t)) - \boldsymbol{J}_j\boldsymbol{\omega}_{j,\mathrm{e}}(t-\tau(t))) \end{cases}$$

and $\boldsymbol{Q}_{i,\mathrm{e}} \triangleq \boldsymbol{Q}_{\mathrm{v}}(\tilde{\boldsymbol{q}}_{i,\mathrm{e}})$, $k_{i,b}$ is the attitude controller gain to be determined.

Denote $\boldsymbol{x}_{i,a}(t) \triangleq \boldsymbol{\eta}_{i,2} + \boldsymbol{\Lambda}_i\boldsymbol{\eta}_{i,1}$, $\boldsymbol{x}_{i,b}(t) \triangleq \boldsymbol{J}_i\boldsymbol{\omega}_{i,\mathrm{e}} + \tilde{\boldsymbol{q}}_{i,\mathrm{e,v}}$, $\boldsymbol{x}_i(t) \triangleq [\boldsymbol{x}_{i,a}^{\mathrm{T}}(t), \boldsymbol{x}_{i,b}^{\mathrm{T}}(t)]^{\mathrm{T}}$, then the overall

closed-loop relative translation and attitude error system is written as

$$\begin{cases}\dot{\boldsymbol{x}}(t)=-\boldsymbol{K}\boldsymbol{x}(t)-\tilde{\boldsymbol{L}}\boldsymbol{x}(t-\tau(t))\\ \boldsymbol{x}(t)=\boldsymbol{\phi}(t)\\ \quad\forall t\in[-\tau_2,-\tau_1]\end{cases}\tag{15}$$

where $\boldsymbol{x}(t)=\boldsymbol{\phi}(t)$ suggests the initial condition, $\boldsymbol{x}(t)\triangleq[\boldsymbol{x}_1^{\mathrm{T}}(t),\boldsymbol{x}_2^{\mathrm{T}}(t),\cdots,\boldsymbol{x}_N^{\mathrm{T}}(t)]^{\mathrm{T}}$, $\tilde{\boldsymbol{L}}\triangleq\tilde{\boldsymbol{L}}\otimes\boldsymbol{I}_{6\times6}$, $\boldsymbol{K}\triangleq\mathrm{diag}\{\boldsymbol{K}_1,\boldsymbol{K}_2,\cdots,\boldsymbol{K}_N\}$, $\boldsymbol{K}_i\triangleq\mathrm{diag}\{k_{i,a},k_{i,b}\}\otimes\boldsymbol{I}_{3\times3}$.

2.2 Exponential stability analysis

Next, sufficient criteria ensuring the exponential stability of closed-loop systems and detailed proof are presented to support the relevant theoretical findings. For simplicity, we denote that $\hbar_r\triangleq\lambda_{\max}\{\boldsymbol{H}_r\},r=1,2,3,4,\kappa_1\triangleq\lambda_{\min}\{\boldsymbol{P}\},\iota\triangleq\iota_1+\iota_2,\kappa_2\triangleq\lambda_{\max}\{\boldsymbol{P}\},\iota_1\triangleq\dfrac{1}{k^2}(\mathrm{e}^{k\tau_2}-k\tau_2-1)\mathrm{e}^{k\tau_2}\hbar_4$,

$$\iota_2\triangleq\kappa_2+\frac{1}{k}(\mathrm{e}^{k\tau_2}(\mathrm{e}^{k\tau_1}-1)\hbar_1+(\mathrm{e}^{k\tau_2}-1)(\hbar_2+\hbar_3)).$$

Theorem 1 Given scalars $\gamma<1$, $k>0$, $0\leqslant\tau_1\leqslant\tau_2$, σ_1, σ_2, and Laplacian matrix $\boldsymbol{L}$, if there exists diagonal matrix $\boldsymbol{P}>0$, matrices $\boldsymbol{H}_r>0$, $r=1,2,3,4$, matrix $\bar{\boldsymbol{K}}$ with proper dimensions, and scalar $\iota>0$, the following inequality (16) holds for $\forall i\in S$.

$$\boldsymbol{\Omega}_k\triangleq\begin{bmatrix}\boldsymbol{\varpi}_{11}&\boldsymbol{\varpi}_{12}&0&\tilde{\boldsymbol{\varpi}}_3\\ *&\boldsymbol{\varpi}_{22}&0&0\\ *&*&-\boldsymbol{H}_1&0\\ *&*&*&\tilde{\boldsymbol{\varpi}}_2\end{bmatrix}<0\tag{16}$$

where

$$\begin{aligned}\boldsymbol{\varpi}_{11}&\triangleq k\boldsymbol{P}-\sigma_1(\bar{\boldsymbol{K}}+\bar{\boldsymbol{K}}^{\mathrm{T}})+\mathrm{e}^{k\tau_2}(\boldsymbol{H}_2+\boldsymbol{H}_3)-\\&\quad 4\mathrm{e}^{k\tau_2}\boldsymbol{H}_4/\tau_2+\mathrm{e}^{k\tau_1}\boldsymbol{H}_1\\ \boldsymbol{\varpi}_1&\triangleq\mathrm{e}^{k\tau_2}(\mathrm{e}^{k\tau_2}-1)\boldsymbol{H}_4/k-2\sigma_2\boldsymbol{P}\\ \boldsymbol{\varpi}_{12}&\triangleq[\boldsymbol{P}-\sigma_1\boldsymbol{P}-\sigma_2\bar{\boldsymbol{K}}^{\mathrm{T}}\quad-\sigma_1\boldsymbol{P}\tilde{\boldsymbol{L}}]\\ \boldsymbol{\varpi}_{22}&\triangleq\begin{bmatrix}\tilde{\boldsymbol{\varpi}}_1&-\sigma_2\boldsymbol{P}\tilde{\boldsymbol{L}}\\ *&-(1-\gamma)\boldsymbol{H}_3\end{bmatrix}\\ \tilde{\boldsymbol{\varpi}}_2&\triangleq\begin{bmatrix}-\boldsymbol{H}_2-4\mathrm{e}^{k\tau_2}\boldsymbol{H}_4/\tau_2&6\mathrm{e}^{k\tau_2}\boldsymbol{H}_4/\tau_2^2\\ *&-12\mathrm{e}^{k\tau_2}\boldsymbol{H}_4/\tau_2^3\end{bmatrix}\\ \tilde{\boldsymbol{\varpi}}_3&\triangleq[-2\mathrm{e}^{k\tau_2}\boldsymbol{H}_4/\tau_2\quad6\mathrm{e}^{k\tau_2}\boldsymbol{H}_4/\tau_2^2]\end{aligned}$$

Then, the error system in Eq.(15) is exponentially stable with controller gains $\boldsymbol{K}\triangleq\mathbf{P}^{-1}\bar{\boldsymbol{K}}$.

Proof Theorem 1 is proved by two steps.

Step 1 The candidate Lyapunov-Krasovskii functional is constructed as

$$V(t)\triangleq\sum_{m=1}^{4}V_m(t)\tag{17}$$

where

$$\begin{aligned}V_1(t)&\triangleq\mathrm{e}^{kt}\boldsymbol{x}^{\mathrm{T}}(t)\boldsymbol{P}\boldsymbol{x}(t)\\ V_2(t)&\triangleq\int_{t-\tau_1}^{t}\mathrm{e}^{k(a+\tau_1)}\boldsymbol{x}^{\mathrm{T}}(\varrho)\boldsymbol{H}_1\boldsymbol{x}(\varrho)\mathrm{d}\varrho+\\&\quad\int_{t-\tau_2}^{t}\mathrm{e}^{k(a+\tau_2)}\boldsymbol{x}^{\mathrm{T}}(\varrho)\boldsymbol{H}_2\boldsymbol{x}(\varrho)\mathrm{d}\varrho\\ V_3(t)&\triangleq\int_{t-\tau(t)}^{t}\mathrm{e}^{k(a+\tau_2)}\boldsymbol{x}^{\mathrm{T}}(\varrho)\boldsymbol{H}_3\boldsymbol{x}(\varrho)\mathrm{d}\varrho\\ V_4(t)&\triangleq\int_{-\tau_2}^{0}\int_{t+z}^{t}\mathrm{e}^{k(a-z+\tau_2)}\dot{\boldsymbol{x}}^{\mathrm{T}}(\varrho)\boldsymbol{H}_4\dot{\boldsymbol{x}}(\varrho)\mathrm{d}\varrho\,\mathrm{d}z\end{aligned}$$

After that, the time-derivative of $V_m(t)$ is deduced that

$$\begin{aligned}\dot{V}_1(t)&=\mathrm{e}^{kt}(k\boldsymbol{x}^{\mathrm{T}}(t)\boldsymbol{P}\boldsymbol{x}(t)+2\boldsymbol{x}^{\mathrm{T}}(t)\boldsymbol{P}\dot{\boldsymbol{x}}(t))\\ \dot{V}_2(t)&=\mathrm{e}^{kt}\boldsymbol{x}^{\mathrm{T}}(t)(\mathrm{e}^{k\tau_1}\boldsymbol{H}_1+\mathrm{e}^{k\tau_2}\boldsymbol{H}_2)\boldsymbol{x}(t)-\\&\quad\mathrm{e}^{kt}\boldsymbol{x}^{\mathrm{T}}(t-\tau_1)\boldsymbol{H}_1\boldsymbol{x}(t-\tau_1)-\\&\quad\mathrm{e}^{kt}\boldsymbol{x}^{\mathrm{T}}(t-\tau_2)\boldsymbol{H}_2\boldsymbol{x}(t-\tau_2)\\ \dot{V}_3(t)&\leqslant-(1-\gamma)\mathrm{e}^{k(t-\tau(t)+\tau_2)}\boldsymbol{x}^{\mathrm{T}}(t-\tau(t))\cdot\\&\quad\boldsymbol{H}_3\boldsymbol{x}(t-\tau(t))+\mathrm{e}^{k(t+\tau_2)}\boldsymbol{x}^{\mathrm{T}}(t)\boldsymbol{H}_3\boldsymbol{x}(t)\\ \dot{V}_4(t)&=\frac{1}{k}\mathrm{e}^{k(t+\tau_2)}(\mathrm{e}^{k\tau_2}-1)\dot{\boldsymbol{x}}^{\mathrm{T}}(t)\boldsymbol{H}_4\dot{\boldsymbol{x}}(t)-\\&\quad\mathrm{e}^{k(t+\tau_2)}\int_{t-\tau_2}^{t}\dot{\boldsymbol{x}}^{\mathrm{T}}(\varrho)\boldsymbol{H}_4\dot{\boldsymbol{x}}(\varrho)\mathrm{d}\varrho\end{aligned}$$

Subsequently, with Lemma 1 in Ref.[20], it finds that

$$\int_{t-\tau_2}^{t}\dot{\boldsymbol{x}}^{\mathrm{T}}(\varrho)\boldsymbol{H}_4\dot{\boldsymbol{x}}(\varrho)\mathrm{d}\varrho\geqslant\frac{2}{\tau_2}\boldsymbol{\delta}^{\mathrm{T}}(t)\boldsymbol{\Theta}\boldsymbol{\delta}(t)\tag{18}$$

where

$$\boldsymbol{\Theta}\triangleq\begin{bmatrix}2\boldsymbol{H}_4&\boldsymbol{H}_4&-3\boldsymbol{H}_4/\tau_2\\ *&2\boldsymbol{H}_4&-3\boldsymbol{H}_4/\tau_2\\ *&*&6\boldsymbol{H}_4/\tau_2^2\end{bmatrix},\boldsymbol{\varsigma}(t)\triangleq\int_{t-\tau_2}^{t}\boldsymbol{x}(\varrho)\mathrm{d}\varrho,$$

and $\boldsymbol{\delta}(t)\triangleq[\boldsymbol{x}^{\mathrm{T}}(t)\quad\boldsymbol{x}^{\mathrm{T}}(t-\tau_2)\quad\boldsymbol{\varsigma}^{\mathrm{T}}(t)]^{\mathrm{T}}$.

Notice that Eq.(19) always holds for all free-weight matrices $\boldsymbol{F}_1\triangleq\sigma_1\boldsymbol{P}$ and $\boldsymbol{F}_2\triangleq\sigma_2\boldsymbol{P}$.

$$\mathrm{sym}\left\{\boldsymbol{\Phi}(t)(\boldsymbol{K}\boldsymbol{x}(t)+\tilde{\boldsymbol{L}}\boldsymbol{x}(t-\tau(t))-\dot{\boldsymbol{x}}(t))\right\}=0\tag{19}$$

where $\boldsymbol{\Phi}(t)\triangleq\boldsymbol{x}^{\mathrm{T}}(t)\boldsymbol{F}_1^{\mathrm{T}}+\dot{\boldsymbol{x}}^{\mathrm{T}}(t)\boldsymbol{F}_2^{\mathrm{T}}$. Define a new variable

$$\boldsymbol{\beta}(t)\triangleq[\boldsymbol{\beta}_1^{\mathrm{T}}(t)\quad\boldsymbol{\beta}_2^{\mathrm{T}}(t)]^{\mathrm{T}}\tag{20}$$

in which

$$\boldsymbol{\beta}_1(t)\triangleq[\boldsymbol{x}^{\mathrm{T}}(t),\dot{\boldsymbol{x}}^{\mathrm{T}}(t),(t-\tau(t))]^{\mathrm{T}}$$

$$\boldsymbol{\beta}_2(t)\triangleq[\boldsymbol{x}^{\mathrm{T}}(t-\tau_1),\boldsymbol{x}^{\mathrm{T}}(t-\tau_2),\boldsymbol{\varsigma}^{\mathrm{T}}(t)]^{\mathrm{T}}$$

Then it is not hard to get the equation $\dot{V}(t)=\mathrm{e}^{kt}\boldsymbol{\beta}^{\mathrm{T}}(t)\boldsymbol{\Omega}_k\boldsymbol{\beta}(t)$.

Additionally, the inequality $\dot{V}(t)<0$ can be guaranteed for $k>0$, which results in

$$V(t)\leqslant V(t_0)+\int_{t_0}^{t}\dot{V}(\varrho)\mathrm{d}\varrho\leqslant V(t_0)\quad t>t_0 \tag{21}$$

Considering Definition 2.1 in Ref.[21], Eq.(17), and Eq.(21), one has $\mathrm{e}^{k(t-t_0)}\kappa_1\boldsymbol{x}^{\mathrm{T}}(t)\boldsymbol{x}(t)\leqslant V(t_0)$, that is

$$\boldsymbol{x}^{\mathrm{T}}(t)\boldsymbol{x}(t)\leqslant\frac{\iota}{\kappa_1}\mathrm{e}^{-k(t-t_0)}\sup_{-\tau_2\leqslant a\leqslant 0}\boldsymbol{x}(\varrho)^{\mathrm{T}}\boldsymbol{x}(\varrho) \tag{22}$$

Thus, we have demonstrated that the error system in Eq.(15) can achieve its exponential stability.

Step 2 Based on the fact $\lim_{t\to\infty}\boldsymbol{x}(t)=\boldsymbol{0}$, more discussion should be added for $\boldsymbol{\eta}_{i,1}$, $\boldsymbol{\eta}_{i,2}$, $\boldsymbol{\omega}_{i,\mathrm{e}}$, and $\tilde{\boldsymbol{q}}_{i,\mathrm{e,v}}$. For this, considering the Lyapunov function

$$V_{i,b}\triangleq\tilde{\boldsymbol{q}}_{i,\mathrm{e,v}}^{\mathrm{T}}\tilde{\boldsymbol{q}}_{i,\mathrm{e,v}}+(1-\tilde{\boldsymbol{q}}_{i,\mathrm{e,c}})^2 \tag{23}$$

and the equation $\boldsymbol{J}_i\boldsymbol{\omega}_{i,\mathrm{e}}+\tilde{\boldsymbol{q}}_{i,\mathrm{e,v}}=\boldsymbol{0}$, one can obtain that

$$\begin{aligned}\dot{V}_{i,b}=&2\tilde{\boldsymbol{q}}_{i,\mathrm{e,v}}^{\mathrm{T}}\dot{\tilde{\boldsymbol{q}}}_{i,\mathrm{e,v}}-2(1-\tilde{\boldsymbol{q}}_{i,\mathrm{e,c}})\dot{\tilde{\boldsymbol{q}}}_{i,\mathrm{e,c}}=\\&\tilde{\boldsymbol{q}}_{i,\mathrm{e,v}}^{\mathrm{T}}(\tilde{\boldsymbol{q}}_{i,\mathrm{e,c}}\boldsymbol{I}_{3\times3}+\tilde{\boldsymbol{q}}_{i,\mathrm{e,v}}^{\times})\boldsymbol{\omega}_{i,\mathrm{e}}+(1-\tilde{\boldsymbol{q}}_{i,\mathrm{e,c}})\tilde{\boldsymbol{q}}_{i,\mathrm{e,v}}^{\mathrm{T}}\boldsymbol{\omega}_{i,\mathrm{e}}=\\&\tilde{\boldsymbol{q}}_{i,\mathrm{e,v}}^{\mathrm{T}}\boldsymbol{\omega}_{i,\mathrm{e}}=-\tilde{\boldsymbol{q}}_{i,\mathrm{e,v}}^{\mathrm{T}}\boldsymbol{J}_i^{-1}\tilde{\boldsymbol{q}}_{i,\mathrm{e,v}}\end{aligned} \tag{24}$$

From Eq.(24), one can conclude that $\lim_{t\to\infty}\tilde{\boldsymbol{q}}_{i,\mathrm{e,v}}=\boldsymbol{0}$ and $\lim_{t\to\infty}\boldsymbol{\omega}_{i,\mathrm{e}}=\boldsymbol{0}$. Similarly, $\lim_{t\to\infty}\boldsymbol{\eta}_{i,1}=\boldsymbol{0}$ and $\lim_{t\to\infty}\boldsymbol{\eta}_{i,2}=\boldsymbol{0}$ can proved by the designed Lyapunov function $V_{i,a}\triangleq\frac{1}{2}\boldsymbol{\eta}_{i,2}^{\mathrm{T}}\boldsymbol{\eta}_{i,2}$, which is omitted here. In summary, the state trajectories of $\boldsymbol{\eta}_{i,1}$, $\boldsymbol{\eta}_{i,2}$, $\boldsymbol{\omega}_{i,\mathrm{e}}$, and $\tilde{\boldsymbol{q}}_{i,\mathrm{e,v}}$ will converge to their equilibrium finally, i.e., all members' flying attitudes and relative positions will track their respective desired values in practice. It finishes the proof.

Remark 1 In closed-loop time-delay systems with exponential convergence, k has a significant impact on control performance and the solvability of the sufficient criteria. To address this issue, one can seek to improve the Lyapunov function and relax the conditions. As a result, a new set of Lyapunov-Krasovskii functional Eq.(17) is developed, which incorporates the bounds and the rate of $\tau(t)$. Meanwhile, the free-weight matrix, as a classic method of analyzing time-delay systems, is utilized. Such two measures together lead to less conservative results.

3 Simulation

In this section, to verify the applicability of controller design, simulation analysis is performed for a gravitational-wave detection mission in LISA, whose orbit and constellation of spacecrafts refer to Fig.2. The inertia matrix $\boldsymbol{J}_i$ ($\mathrm{kg\cdot m^2}$) for C_i is given as

$$\begin{aligned}\boldsymbol{J}_1&=\mathrm{diag}\{50.75,51.00,49.25\}\\\boldsymbol{J}_2&=\mathrm{diag}\{60.50,54.50,52.50\}\\\boldsymbol{J}_3&=\mathrm{diag}\{47.75,51.50,51.00\}\end{aligned}$$

The weights of the directed edges are $\alpha_{13}=1$, $\alpha_{21}=1$, and $\alpha_{32}=1$. The communication delays are $\tau(t)=8.3+0.2\mathrm{e}^t/(1+\mathrm{e}^t)$ s. Furthermore, given scalars $\tau_1=8.3$, $\tau_2=8.5$, $k=0.02$, $\gamma=0.05$, and $\sigma_1=\sigma_2=1$, the controller gains is computed by sufficient criteria in Theorem 1 as $\boldsymbol{K}=1.991\boldsymbol{I}_{18\times18}$. For $i\in S$, $\boldsymbol{\Lambda}_i=0.012\boldsymbol{I}_{3\times3}$. Besides, the initial states of $\tilde{\boldsymbol{q}}_i$, $\boldsymbol{\omega}_i$ (rad/s), $\boldsymbol{\eta}_{i,1}$(m), and $\boldsymbol{\eta}_{i,2}$ (m/s) are chosen as follows

$$\begin{aligned}\tilde{\boldsymbol{q}}_1(0)&=[-0.1,0.5,-0.01,0.860\,2]^{\mathrm{T}}\\\tilde{\boldsymbol{q}}_2(0)&=[0.6,-0.1,0.3,0.734\,8]^{\mathrm{T}}\\\tilde{\boldsymbol{q}}_3(0)&=[0.5,0.6,0.1,0.616\,4]^{\mathrm{T}}\\\boldsymbol{\eta}_{1,2}(0)&=[0.03,-0.06,0.02]^{\mathrm{T}}\\\boldsymbol{\eta}_{2,2}(0)&=[-0.03,0.03,0.05]^{\mathrm{T}}\\\boldsymbol{\eta}_{3,2}(0)&=[0.05,0.08,-0.02]^{\mathrm{T}}\\\boldsymbol{\eta}_{1,1}(0)&=[1.7,1.8,-1.5]^{\mathrm{T}}\times10^3\\\boldsymbol{\eta}_{2,1}(0)&=\left[\sqrt{3},1.5,-1.5\right]^{\mathrm{T}}\times10^3\\\boldsymbol{\eta}_{3,1}(0)&=[-1.6,1.5,-1.8]^{\mathrm{T}}\times10^3\\\boldsymbol{\omega}_1(0)&=[0.01,0.03,-0.02]^{\mathrm{T}}\\\boldsymbol{\omega}_2(0)&=[0.01,-0.01,0.01]^{\mathrm{T}}\\\boldsymbol{\omega}_3(0)&=[0.01,0.03,-0.01]^{\mathrm{T}}\end{aligned}$$

In O_{L}, the desired configuration parameters $\boldsymbol{p}_{i,\mathrm{d}}$ (m), $\dot{\boldsymbol{p}}_{i,\mathrm{d}}$ (m/s) and $\ddot{\boldsymbol{p}}_{i,\mathrm{d}}$ ($\mathrm{m/s^2}$) are designed as

$$\begin{aligned}\boldsymbol{p}_{1,\mathrm{d}}(0)=&[721\,621\,546.00,-19\,562\,993.95,\\&1\,249\,792\,164.00]^{\mathrm{T}}\\\boldsymbol{p}_{2,\mathrm{d}}(0)=&[-352\,186\,249.80,1\,259\,838\,369.00,\\&-609\,992\,643.50]^{\mathrm{T}}\end{aligned}$$

$$\boldsymbol{p}_{3,\mathrm{d}}(0)=[-369\,296\,490.50,\ -1\,240\,086\,183.00,\ -582\,521\,513.30]^{\mathrm{T}}$$

$$\dot{\boldsymbol{p}}_{1,\mathrm{d}}(0)=[-1.947\,4,\ -287.905\,3,\ -3.364\,8]^{\mathrm{T}}$$

$$\dot{\boldsymbol{p}}_{2,\mathrm{d}}(0)=[125.401\,0,139.881\,0,217.196\,4]^{\mathrm{T}}$$

$$\dot{\boldsymbol{p}}_{3,\mathrm{d}}(0)=[-123.443\,8,139.881\,0,217.196\,4]^{\mathrm{T}}$$

$$\ddot{\boldsymbol{p}}_{1,\mathrm{d}}(0)=[0.005\,9,\ -7.630\,0\times10^{-7},\ 4.880\,0\times10^{-5}]^{\mathrm{T}}$$

$$\ddot{\boldsymbol{p}}_{2,\mathrm{d}}(0)=[0.006\,0,5.022\,0\times10^{-5},\ -2.430\,0\times10^{-5}]^{\mathrm{T}}$$

$$\ddot{\boldsymbol{p}}_{3,\mathrm{d}}(0)=[0.006\,0,\ -4.950\,0\times10^{-5},\ -2.550\,0\times10^{-5}]^{\mathrm{T}}$$

Then, with the presented attitude-orbit coordinated controller in Eqs.(13—14), the time response of closed-loop relative translation and attitude error system in Eq.(15) are displayed in Figs.3,4. These results show that the state trajectories of the closed-loop error system in Eq.(15) can converge with high precision to some degree. Therein, $\eta_{i,1}^{s}$ $(s=1,2,3)$ stands for the sth element of $\boldsymbol{\eta}_{i,1}$. After $t=5\,000$ s, the state trajectories of relative position and attitude errors can remain in the regions $|\eta_{i,1}^{s}|<0.92$ m and $|\tilde{q}_{i,\mathrm{e,v}}^{s}|<1\times10^{-5}$, respectively. Meanwhile, the time response of attitude-orbit control input is shown in Fig.5, from which one can find that the state trajectories of input accelerations and torques are rapidly driven into the areas $|u_{i,a}^{s}|<5\times10^{-3}$ m/s^2 and $|u_{i,b}^{s}|<5\times10^{-2}$ N·m within $t=100$ s, respectively. In addition, from Fig.6, the state trajectories of desired attitude $\tilde{\boldsymbol{q}}_{i,\mathrm{d}}$ of C_i is time-invariant because three spacecrafts finally keep relatively static as an ultra-stable platform, and the curves of attitude $\tilde{q}_i^{s}$ can smoothly and rapidly track their desired values when suffering from large-scale communication delays.

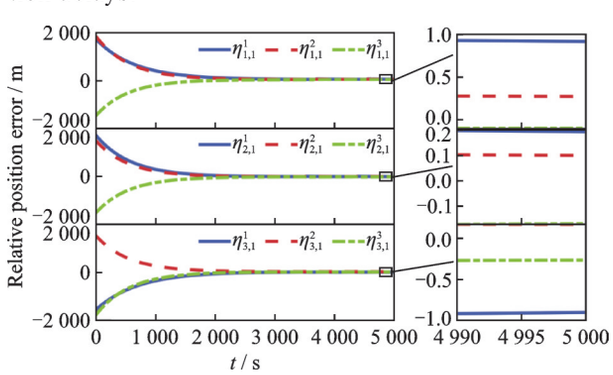

Fig.3 Time response of $\boldsymbol{\eta}_{i,1}$

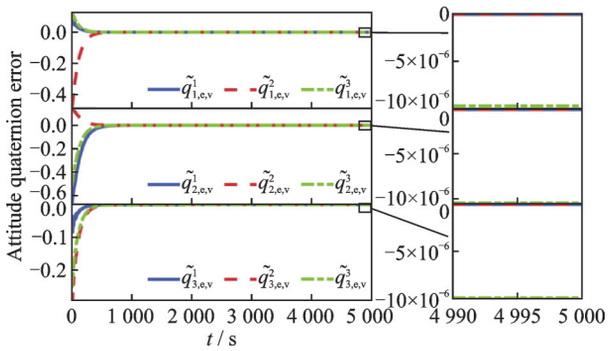

Fig.4 Time response of $\tilde{\boldsymbol{q}}_{i,\mathrm{e,v}}$

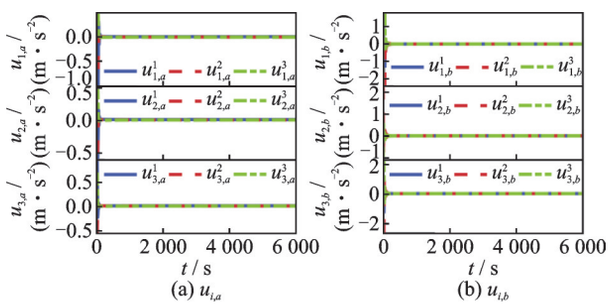

Fig.5 Time response of $\boldsymbol{u}_{i,a}$ and $\boldsymbol{u}_{i,b}$

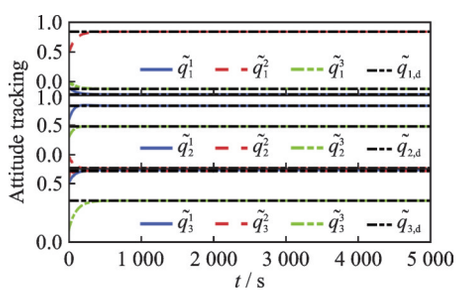

Fig.6 Time response of attitude tracking

As a comparison, a robust coordinated controller in Eq.(25) stated in Ref.[22] is used in this section. First, denote an auxiliary error variable $\boldsymbol{s}_i\triangleq\epsilon_i\boldsymbol{x}_{i,1}+\boldsymbol{x}_{i,2}$, with $\boldsymbol{x}_{i,1}\triangleq[\boldsymbol{\eta}_{i,1}^{\mathrm{T}},\tilde{\boldsymbol{q}}_{i,\mathrm{e,v}}^{\mathrm{T}}]^{\mathrm{T}}$ and $\boldsymbol{x}_{i,2}\triangleq[\boldsymbol{\eta}_{i,2}^{\mathrm{T}},\boldsymbol{\omega}_{i,\mathrm{e}}^{\mathrm{T}}]^{\mathrm{T}}$, then

$$\boldsymbol{u}_{i,\mathrm{c}}\triangleq-k_{\mathrm{s},i}\upsilon_i\sum_{j=1}^{N}\Big(\alpha_{ij}(\boldsymbol{s}_i-\boldsymbol{s}_j(t-\tau(t)))+b_i\boldsymbol{s}_i\Big) \tag{25}$$

$$\upsilon_i\triangleq\begin{cases}\epsilon_i\left(1+\dfrac{\|\boldsymbol{s}_i\|}{\sinh(\|\boldsymbol{s}_i\|)}\right) & \|\boldsymbol{s}_i\|\neq0\\ 2\epsilon_i & \text{Otherwise}\end{cases} \tag{26}$$

where $b_i>0$ is the weighted adjacent coefficient with C_0, and other scalars $k_{\mathrm{s},i}>0$, $\epsilon_i>0$, $\varepsilon_i>0$ are constants for $\forall i\in S$.

With the same orbit and attitude parameters in the context and the controller in Eq.(25), the simulations are plotted in Figs.7—9. From Fig.7, the convergence of relative position $\boldsymbol{\eta}_{i,1}$ exhibits larger

steady-state errors. From Figs.8,9, the convergence of attitude error $\tilde{\boldsymbol{q}}_{i,\mathrm{e,v}}$ and attitude tracking cannot achieve fast convergence. Compared with the attitude-orbit coordinated controller in Eqs.(13—14), it is hard for the controller in Eq.(25) to deal with large-scale communication delays $\tau(t)$ such that the lowly precise control performance is achieved.

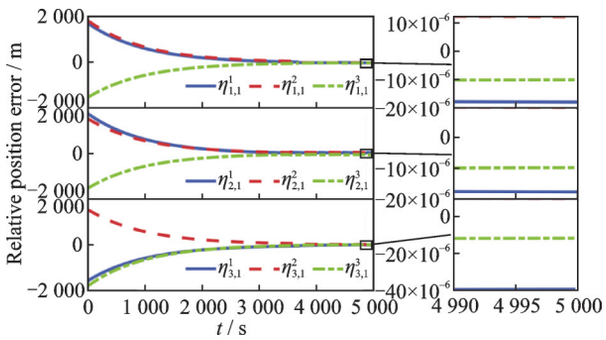

Fig.7 Time response of $\boldsymbol{\eta}_{i,1}$ with controller in Ref. [22]

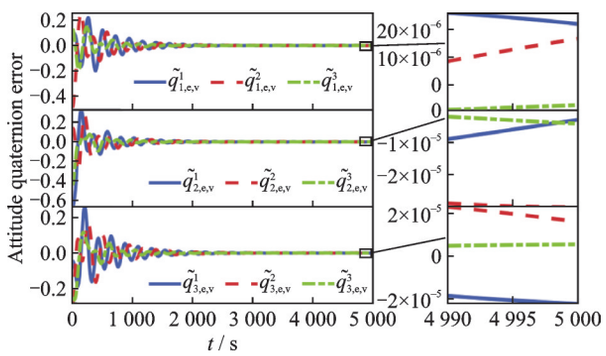

Fig.8 Time response of $\tilde{\boldsymbol{q}}_{i,\mathrm{e,v}}$ with controller in Ref.[22]

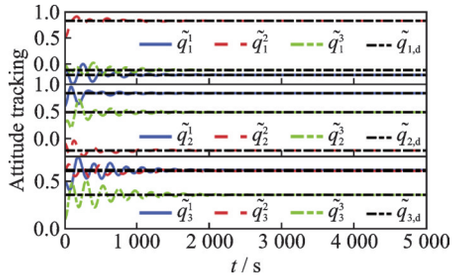

Fig.9 Time response of attitude tracking with controller in Ref.[22]

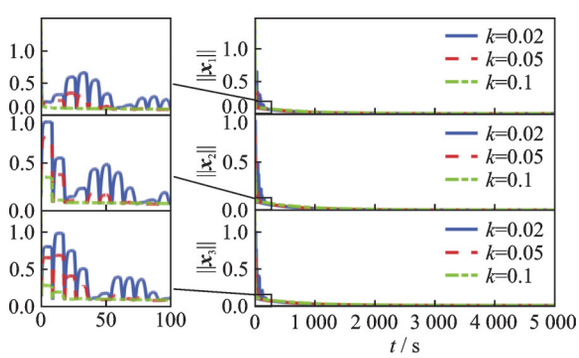

Fig.10 Time response of $\|\boldsymbol{x}_i\|$ with different values of k

Furthermore, to illustrate the trend of arm length variation in the gravitational wave detection formation flying, we present Fig.11, which visually demonstrates how the actual arm length tracks the desired value under the influence of the proposed controller. L_{12}, L_{23} and L_{31} represent the three arm lengths of the spacecraft formation configuration.

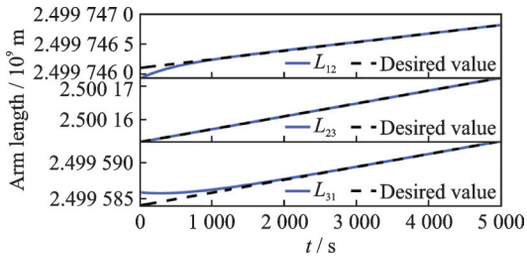

Fig.11 Variation in arm length of the gravitational wave detection formation

The flexibility and superiority of the proposed method can be analyzed from both theoretical and simulation aspects. In theory, the tracking error system in Ref.[22] is proved to be globally stable while the exponential stability of the closed-loop time-delay system in Eq.(15) is achieved in the Lyapunov sense. In practice, one can stabilize the tracking error system in Eq.(15) with a fast convergence by adjusting k. In simulation, Fig.10 shows the time responses of $\|\boldsymbol{x}_i\|$ with different values of k. Note that k plays a critical role in control performance and the solvability of the sufficient criteria. With other conditions being fixed, the larger values of k make the faster convergence of the tracking errors. Besides, it finds that the solvability of the proposed results remains reliable even with different candidate values of k, which means that the proposed method is flexible to some degree.

Furthermore, the energy cost index (ECI) is defined as

$$\mathrm{ECI}=\int_0^t(\boldsymbol{u}_i^{\mathrm{T}}(l)\boldsymbol{u}_i(l))^{\frac{1}{2}}\mathrm{d}l \tag{27}$$

Then, we can quantize the ECI of formation flying under different methods and show it in Fig.12. As a conclusion, with the large-scale communication delays, the tracking error system can achieve better control performance but less energy cost by an exponential attitude-orbit coordinated controller, which illustrates the superiority of the proposed method.

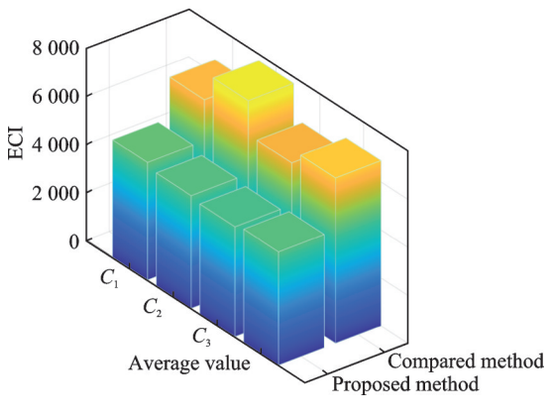

Fig.12 ECI of formation flying under different methods

4 Conclusions

This paper studies the exponential delayed attitude-orbit coordinated control problems for gravitational-wave detection spacecraft formation. Due to the oversized formation configuration, the large-scale communication delays are modeled. Meanwhile, a new delay-dependent attitude-orbit coordinated controller is designed. Furthermore, sufficient criteria ensuring the exponential stability of the closed-loop delayed system are derived. Finally, simulation results demonstrate the effectiveness of the proposed control scheme.

References

[1] GONG Y G, LUO J, WANG B. Concepts and status of Chinese space gravitational wave detection projects[J]. Nature Astronomy, 2021, 5: 881-889.

[2] BAILES M, BERGER B K, BRADY P R, et al. Gravitational-wave physics and astronomy in the 2020s and 2030s[J]. Nature Reviews Physics, 2021, 3: 344-366.

[3] WANG W, WU D, HEXI B Y. Fuel-optimal control for multiple spacecraft formation flying with relative motion constraints[J]. IEEE Transactions on Aerospace and Electronic Systems, 2024, 60(6): 8569-8582.

[4] KRÓLAK A, PATIL M. The first detection of gravitational waves[J]. Universe, 2017, 3(3): 59.

[5] CAPRINI C, CHALA M, DORSCH G C, et al. Detecting gravitational waves from cosmological phase transitions with LISA: An update[J]. Journal of Cosmology and Astroparticle Physics, 2020(3): 1-58.

[6] YANG C H, ZHANG H. Formation flight design for a LISA-like gravitational wave observatory via cascade optimization[J]. Astrodynamics, 2019, 3(2): 155-171.

[7] KAWAMURA S, NAKAMURA T, ANDO M, et al. The Japanese space gravitational wave antenna: DECIGO[J]. Classical and Quantum Gravity, 2007, 23: 125-131.

[8] LUO J, CHEN L S, DUAN H Z, et al. TianQin: A space-borne gravitational wave detector[J]. Classical and Quantum Gravity, 2016, 33(3): 035010.

[9] TORRES-ORJUELA A, HUANG S J, LIANG Z C, et al. Detection of astrophysical gravitational wave sources by TianQin and LISA[J]. Science China Physics, Mechanics & Astronomy, 2024, 67(5): 259511.

[10] HU W R, WU Y L. The TaiJi Program in Space for gravitational wave physics and the nature of gravity[J]. National Science Review, 2017, 4(5): 685-686.

[11] SHI Y X, HU Q L, LI D Y, et al. Adaptive optimal tracking control for spacecraft formation flying with event-triggered input[J]. IEEE Transactions on Industrial Informatics, 2023, 19(5): 6418-6428.

[12] SONG Y, PARK S Y, LEE S, et al. Spacecraft formation flying system design and controls for four nanosats mission[J]. Acta Astronautica, 2021, 186: 148-163.

[13] WANG W J, LI C J, GUO Y N. Relative position coordinated control for spacecraft formation flying with obstacle/collision avoidance[J]. Nonlinear Dynamics, 2021, 104(2): 1329-1342.

[14] ZHANG J, HU Q L, WANG D W, et al. Robust attitude coordinated control for spacecraft formation with communication delays[J]. Chinese Journal of Aeronautics, 2017, 30(3): 1071-1085.

[15] DENG C, CHE W W, WU Z G. A dynamic periodic event-triggered approach to consensus of heterogeneous linear multiagent systems with time-varying communication delays[J]. IEEE Transactions on Cybernetics, 2021, 51(4): 1812-1821.

[16] GONG S Q, GUO Z Y, WEN S P. Finite-time synchronization of T-S fuzzy memristive neural networks with time delay[J]. Fuzzy Sets and Systems, 2023, 459: 67-81.

[17] ZHANG Y, LIU Y, YANG J K, et al. Attitude-orbit coupled control of gravitational wave detection spacecraft with communication delays[J]. Sensors, 2023, 23(6): 3233.

[18] JIN E D, SUN Z W. Robust controllers design with finite time convergence for rigid spacecraft attitude tracking control[J]. Aerospace Science and Technology, 2008, 12(4): 324-330.

[19] SHAO X D, HU Q L, SHI Y, et al. Fault-tolerant control for full-state error constrained attitude tracking of uncertain spacecraft[J]. Automatica, 2023, 151: 110907.

[20] SHEN H, SU L, PARK J H. Reliable mixed H_∞/passive control for T-S fuzzy delayed systems based on a semi-Markov jump model approach[J]. Fuzzy Sets and Systems, 2017, 314: 79-98.

[21] CAO J W. Improved delay-dependent exponential stability criteria for time-delay system[J]. Journal of the Franklin Institute, 2013, 350(4): 790-801.

[22] ZHU Z H, GUO Y. Robust adaptive attitude tracking coordination control for spacecraft formation with unknown time-varying inertia[J]. Proceedings of the Institution of Mechanical Engineers, Part G: Journal of Aerospace Engineering, 2019, 233(1): 310-323.

Acknowledgements This work was supported by the National Key R&D Program of China (No.2022YFC2204800) and the Graduate Student Independent Exploration and Innovation Program of Central South University (No.2024ZZTS 0767).

Authors

The first author Mr. **XING Youpeng** received his B.S. degree in intelligence science and technology from Central South University, Changsha, China, in 2021. His current research interests include nonlinear spacecraft relative motion dynamics, prescribed performance control, optimal control, and their applications in on-orbit tasks.

The corresponding author Dr. **YIN Zeyang** received his B.S. and Ph.D. degrees from School of Astronautics, Northwestern Polytechnical University, Xi'an, China, in 2014 and 2020, respectively. From 2017 to 2018, he was a joint training Ph.D. student with Department of Mechanical Engineering, University of Victoria, Canada. He is currently an associate professor with School of Automation, Central South University, Changsha, China. His research interests include the intelligent decision, optimization, and control of unmanned systems.

Author contributions Mr. **XING Youpeng** complied the models, conducted the analysis, derived the proposed method, and wrote the manuscript. Mr. **SONG Yinsheng** conducted the validation and visualization. Dr. **YIN Zeyang** designed and supervised the study, and revised the manuscript. Prof. **CHEN Xiaofang** supervised the study and revised the manuscript. All authors commented on the manuscript draft and approved the submission.

Competing interests The authors declare no competing interests.

(Production Editor: ZHANG Bei)

考虑大尺度通信时延的引力波探测航天器编队指数收敛姿轨协同控制

邢友朋，宋寅生，殷泽阳，陈晓方

（中南大学自动化学院，长沙 410083，中国）

摘要：研究了引力波探测编队航天器系统的指数收敛姿轨协同控制问题。首先，对天基激光干涉仪星间距离过大导致的大规模通信时延进行了建模。然后，面向通信时延的影响，设计了一种基于时延信息的姿轨协同控制器。此外，通过重建保守性较小的Lyapunov-Krasovskii函数和自由权重矩阵，推导出保证闭环相对位姿误差系统指数稳定的充分条件。最后，通过仿真算例验证了设计的控制器在引力波探测任务中的有效性。

关键词：引力波探测；航天器编队；姿轨协同控制；大规模通信时延；指数稳定性